Supporting information

The potassium energy storage behavior of Nickel-Znic co-doped Prussian blue analogs formed by a chelating agent assisted route and its application in a K^+-proton hybrid ions aqueous alkaline Battery

Ruiqing Hua[a], Caiyun Xu[a], Dian Lin[a], Deyu Qu[a*], Xi Li[a], Ruiming Zhang[c], Zhizhong Xie [a*], Haolin Tang[b,d], Junsheng Li[a,d], Dan Liu[a,c *]

[a] *Department of Chemistry, School of Chemistry, Chemical Engineering and Life Science, Wuhan University of Technology, 122 Luoshi Road, Wuhan 430070, Hubei, P.R. China*

[b] *State Key Laboratory of Advanced Technology for Material Synthesis and Processing, School of Materials Science and Engineering, Wuhan University of Technology, 122 Luoshi Road, Wuhan 430070, Hubei, P.R. China*

[c] *Foshan Xianhu Laboratory of the Advanced Energy Science and Technology Guangdong Laboratory, Xianhu Hydrogen Valley, Foshan 528200, China*

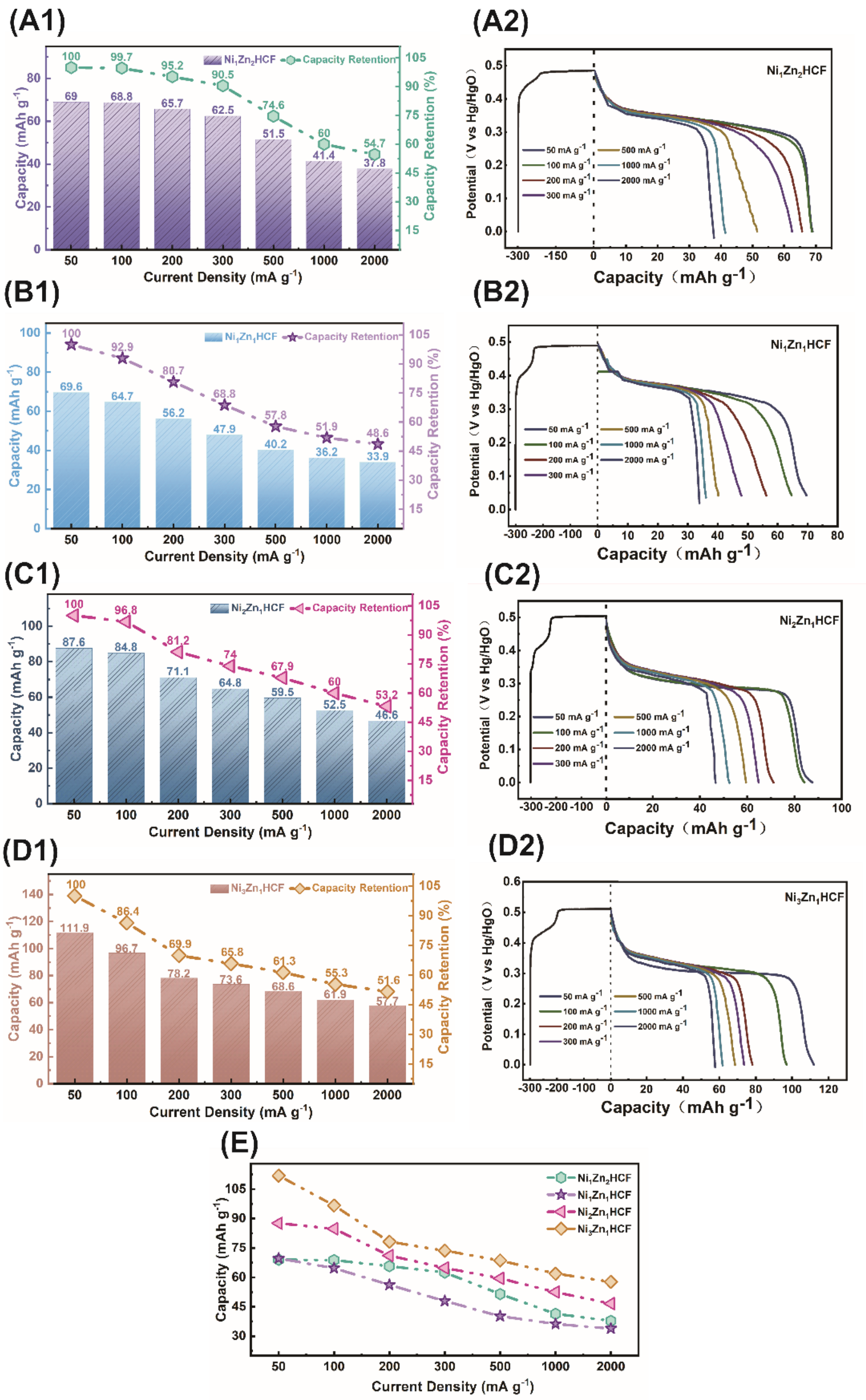

Fig.S1. Rate performances of Ni_xZn_yHCF electrodes. (A1)(A2): Ni_1Zn_2HCF. (B1)(B2): Ni_1Zn_1HCF. (C1)(C2): Ni_2Zn_1HCF. (D1)(D2): Ni_3Zn_1HCF. (E) the comparison of Ni_xZn_yHCF electrodes.

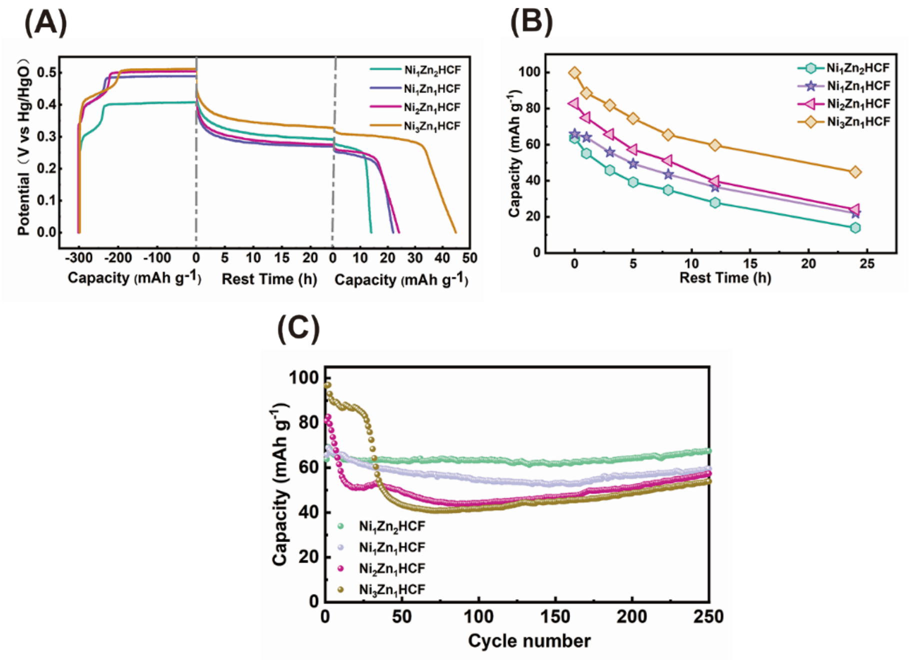

Fig.S2. （A）Open-circuit potential profiles and charge-discharge curves under an applied current density of 100 mA g^{-1} after charging the electrode for 3 h in 30 wt% KOH solution followed by 24 h at open circuit potential. (B) Discharge capacities after resting at various of time. (C) Cyclic performances of the Ni_xZn_yHCF electrodes.

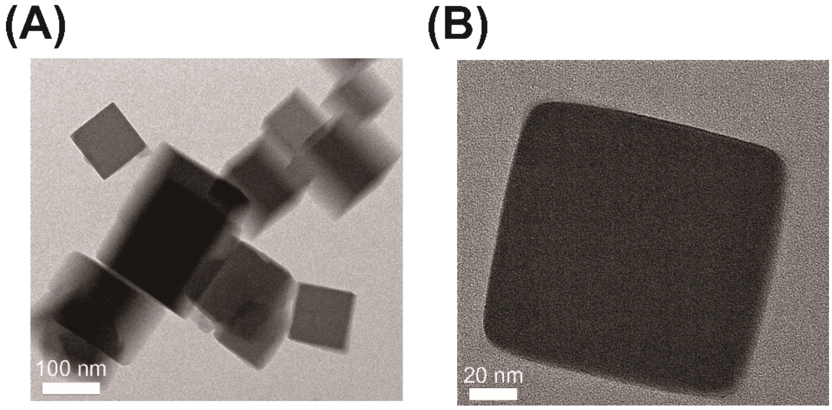

Fig.S3. TEM images of Ni_3Zn_1HCF-10.

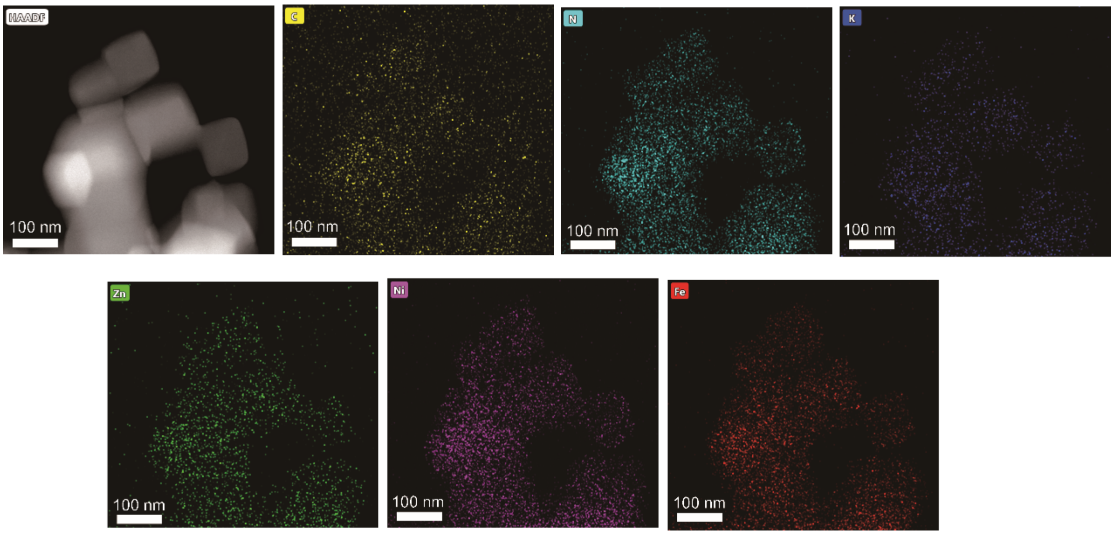

Fig.S4. Energy-dispersive spectroscopic (EDS) elemental mapping images of Ni_3Zn_1HCF-10.

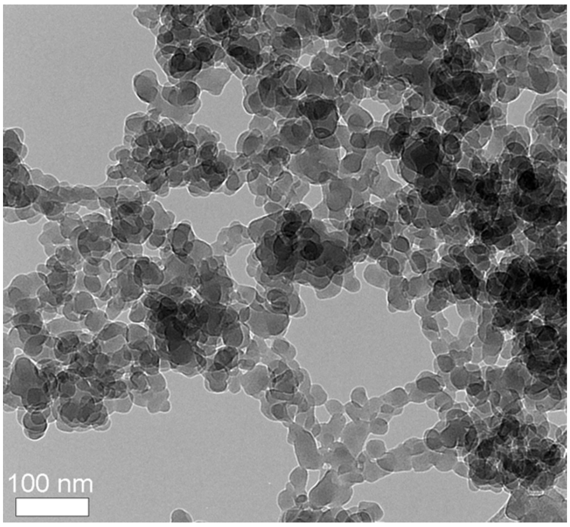

Fig.S5. TEM image of Ni_3Zn_1HCF.

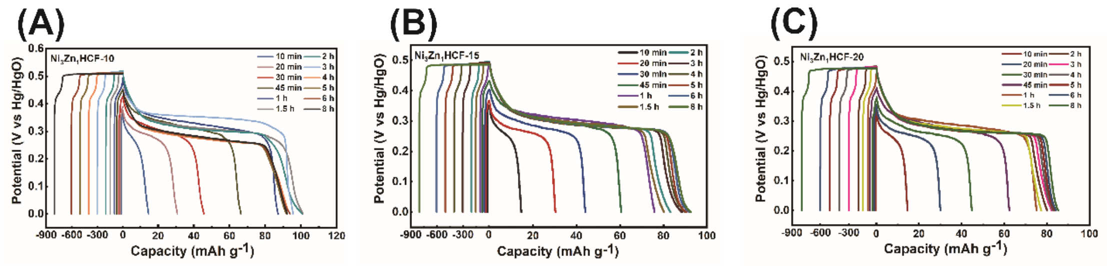

Fig.S6. Charge and discharge curves of Ni_3Zn_1HCF-Z (Z=10,15,20) electrodes after being charge for various time.

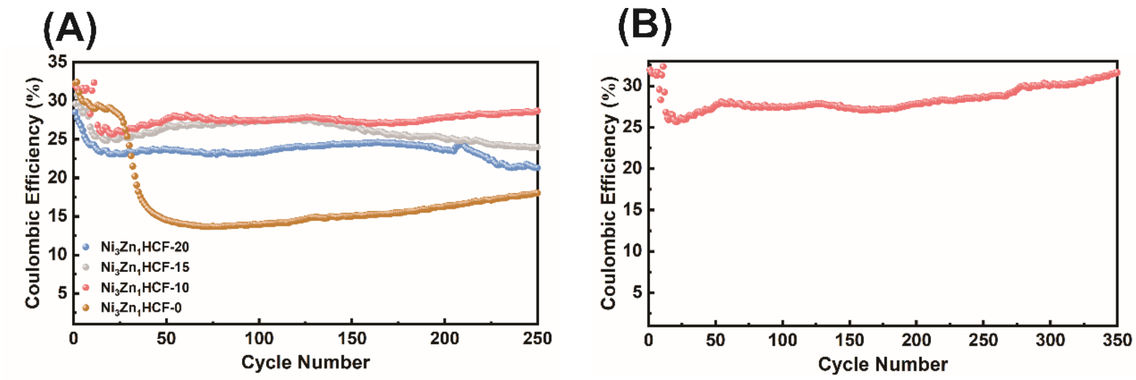

Fig.S7. (A) Coulombic efficiencies of Ni_3Zn_1HCF-Z electrode (Z=0,10,15,20) under 100 mA g^{-1} (250 cycles). (B) Coulombic efficiencies of Ni_3Zn_1HCF-10 electrode under 100 mA g^{-1} (350 cycles).

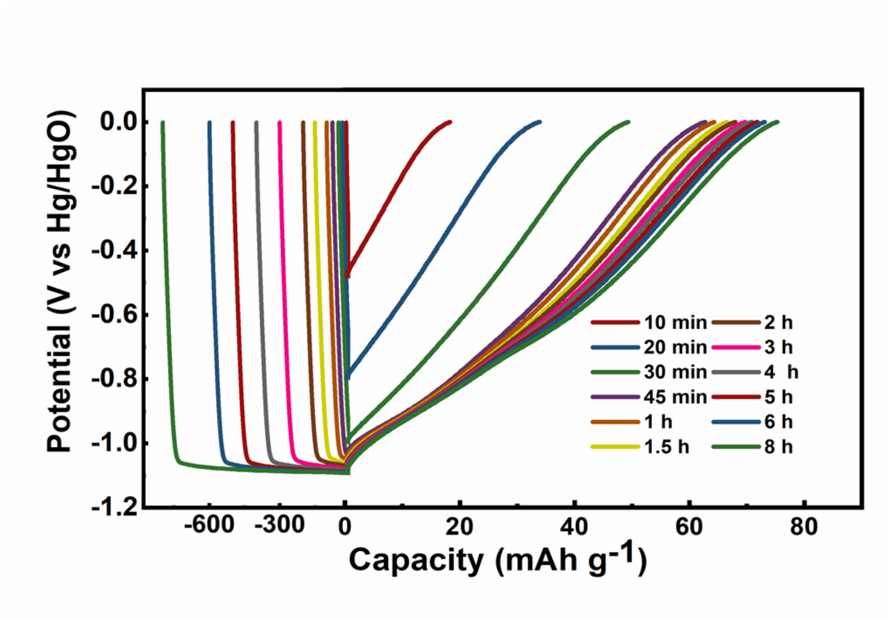

Fig.S8. Charge and discharge curves of AC electrode after being charge for various time.

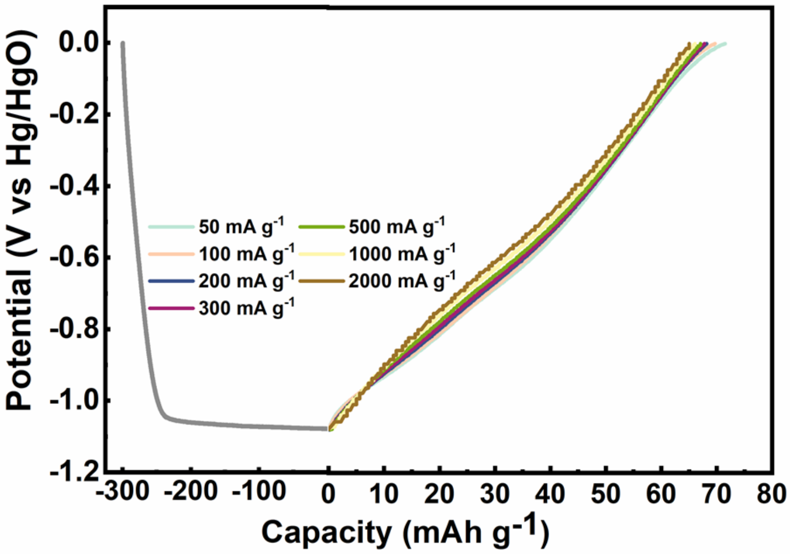

Fig.S9. Rate performance of AC.

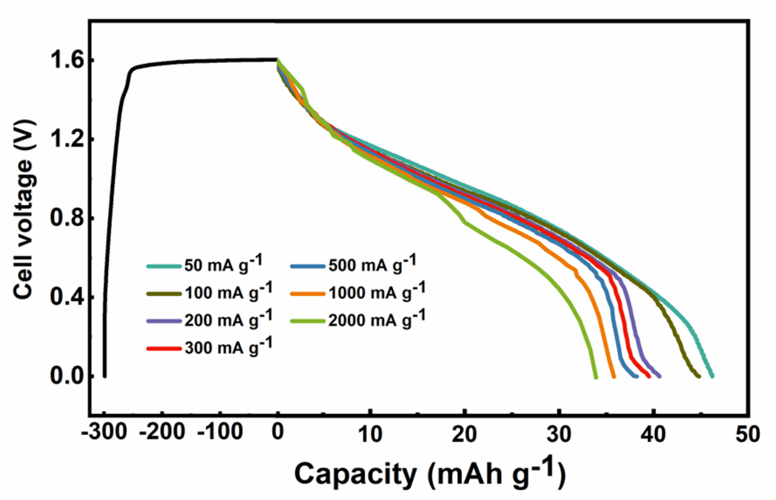

Fig.S10. Rate performance of the full cell.

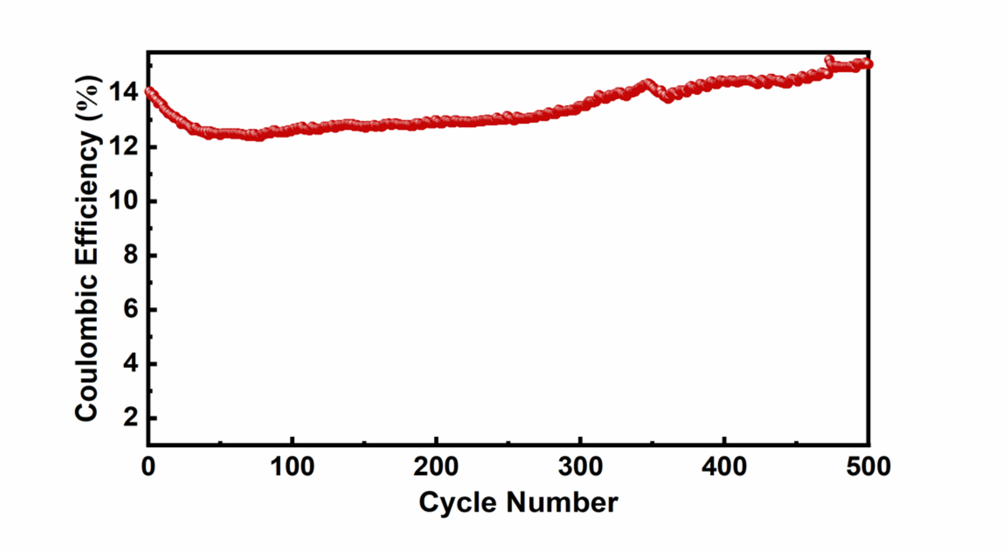

Fig.S11. Coulombic efficiencies of full cell under 100 mA g^{-1} (500 cycles).

Table S1: The electrode performance comparison of our work and other aqueous batteries reported previously.

Cathode material	Electrolyte	Rate capability	Initial capacity	Cyclability	Ref.
CuHCF	$Al_2(SO_4)_3$	74% capacity retention (30.3 mAh g^{-1})	41 mAh g^{-1}	1000 cycles, 54.9%	Ref [1]
PB	$NaSO_4$	68% capacity retention (34.5 mAh g^{-1})	50 mAh g^{-1}	200 cycles, 84%	Ref [2]
NiHCF	$ZnSO_4$	52% capacity retention(35 mAh g^{-1})	67 mAh g^{-1}	100 cycles, 87%	Ref [3]
MgFeHCF	$FeSO_4$	75% capacity retention (65 mAh g^{-1})	86 mAh g^{-1}	500 cycles, 70.9 %	Ref [4]
This work	KOH	52.9% capacity retention(50.5 mAh g^{-1})	95.5 mAh g^{-1}	350 cycles, 99.9%	

Reference:

[1] S. Liu, G.L. Pan, G.R. Li, X.P. Gao, *J. Mater. Chem. A*, 2015, **3**, 959-962.

[2] A.J. Fernández-Ropero, M.J. Piernas-Muñoz, E. Castillo-Martínez, T. Rojo, M. Casas-Cabanas, *Electrochim. Acta*, 2016, **210**, 352-357.

[3] Z. Li, T. Liu, R. Meng, L. Gao, Y. Zou, P. Peng, Y. Shao, X. Liang, *Energy Environ. Mater.*, 2020, **4**, 111-116.

[4] G. Huang, Z. Lao, Z. He, F. Xiong, S. Tan, M. Huang, G. Thompson, Q. An, L. Mai, *Chem. Commun.*, 2023, **59**, 4067-4070.

Table S2: ICP-OES, inductively coupled plasma optical emission spectrometry.

Material	Elements contents (%)					Chemical formula
	K	Ni	Zn	Fe	H_2O	
Ni_1Zn_2HCF	0.44	5.68	12.13	12.45	20.64	$K_{0.04}Ni_{0.33}Zn_{0.66}[Fe(CN)_6]_{0.80}$•$□_{0.20}$•4.12$H_2O$
Ni_1Zn_1HCF	1.21	10.8	9.66	12.97	`17.83	$K_{0.11}Ni_{0.5}Zn_{0.5}[Fe(CN)_6]_{0.79}$•$□_{0.21}$•4.47 H_2O
Ni_2Zn_1HCF	1.14	6.63	13.79	13.01	19.73	$K_{0.1}Ni_{0.66}Zn_{0.33}[Fe(CN)_6]_{0.76}$•$□_{0.24}$•3.70$H_2O$
Ni_3Zn_1HCF	1.24	15.15	4.96	13.27	24.21	$K_{0.1}Ni_{0.75}Zn_{0.25}[Fe(CN)_6]_{0.78}$•$□_{0.22}$•4.43$H_2O$

The composition and formula of Ni_1Zn_2HCF, Ni_1Zn_1HCF and Ni_2Zn_1HCF samples are also evaluated along with the Ni_3Zn_1HCF which summarized in the table S2. It is found that the amount of $[Fe(CN)_6]$ vacancies are relatively similar among them. Meantime, the Ni_3Zn_1HCF sample has the highest content of crystal H_2O among the four samples. Since the existing of crystal water may jeopardize the capacity of PBA and Ni_3Zn_1HCF sample has the highest capacity among the four samples, the observed electrochemical behaviors difference between Ni_1Zn_2HCF, Ni_1Zn_1HCF, Ni_2Zn_1HCF and Ni_3Zn_1HCF samples may be mainly due to different Ni to Zn ratios in the samples. The effects of vacancies and crystal water upon the electrochemical performances may become significant when the samples have the same ratio of Ni to Zn, as demonstrated between the Ni_3Zn_1HCF-10 and Ni_3Zn_1HCF-0 materials.